Thermal stress analysis and supercontinuum generation in germanate-tellurite composite fibers

Mathieu Boivin, Mohammed El-Amraoui, Yannick Ledemi, Fabrice Célarié, Réal Vallée, Younes Messaddeq

Thermal stress analysis and supercontinuum generation in germanate-tellurite composite fibers

Mathieu Boivin,[1*] Mohammed El-Amraoui,[1] Yannick Ledemi,[1] Fabrice Célarié,[2] Réal Vallée,[1] and Younès Messaddeq[1]

[1]*Center for Optics, Photonics and Lasers (COPL), Université Laval, Québec, G1V 0A6, Canada*

[2]*Institut de Physique de Rennes, Université de Rennes 1, Rennes, UMR CNRS 6251, France*

[*]*mathieuboivin2@gmail.com*

Abstract: The build-up of thermal stress inside germanate-tellurite composite preforms prepared by a modified built-in casting technique was quantitatively evaluated with a theoretical model. This analysis has shown that for particular combinations of tellurite glass-made core and germanate-tellurite glass-made cladding, accumulations of thermal stress in extension and in compression occur over two different temperature ranges during the cooling of the preforms toward ambient temperature. When the glass properties are appropriate, these two regimes of stress accumulation can counterbalance each other in order to achieve a moderate structural stress inside the composite preforms. The composite fibers drawn from these preforms were then pumped with a mode-locked fiber laser centered at 1.91 μm to assess their potential for supercontinuum generation in the infrared.

OCIS codes: (190.4400) Nonlinear optics, materials; (190.4370) Nonlinear optics, fibers; (060.2280) Fiber design and fabrication; (060.2290) Fiber materials; (060.2390) Fiber optics, infrared.

References and links

1. D. M. Brown, K. Shi, Z. Liu, and C. R. Philbrick, "Long-path supercontinuum absorption spectroscopy for measurement of atmospheric constituents," Opt. Express **14,** 8457–8471 (2008).
2. C. R. Petersen, U. Møller, I. Kubat, B. Zhou, S. Dupont, J. Ramsay, T. Benson, S. Sujecki, N. Abdel-Moneim, Z. Tang, D. Furniss, A. Seddon, and O. Bang, " Mid-infrared supercontinuum covering the 1.4–13.3 μm molecular fingerprint region using ultra-high NA chalcogenide step-index fibre," Nat. Photonics **8,** 830–834 (2014).
3. H. H. P. Th. Bekman, J. C. van den Heuvel, F. J. M. van Putten, and H. M. A. Schleijpen, " Development of a mid-infrared laser for study of infrared countermeasures techniques," Proc. SPIE **5615,** 27–38 (2004).
4. D. H. Titterton, *Military Laser Technology and Systems* (Artech House, 2015).
5. J. M. Dudley, G. Genty, and S. Coen " Supercontinuum generation in photonic crystal fiber," Rev. Mod. Phys. **78,** 1135–1184 (2006).
6. C. Xia, M. Kumar, O. P. Kulkarni, M. N. Islam, F. L. Terry Jr., M. J. Freeman, M. Poulain, and G. Mazé, "Mid-infrared supercontinuum generation to 4.5 μm in ZBLAN fluoride fibers by nanosecond diode pumping," Opt. Lett. **31,** 2553–2555 (2006).
7. I. Savelii, O. Mouawad, J. Fatome, B. Kibler, F. Désévédavy, G. Gadret, J.-C. Jules, P.-Y. Bony, H. Kawashima, W. Gao, T. Kohoutek, T. Suzuki, Y. Ohishi, and F. Smektala, "Mid-infrared 2000-nm bandwidth supercontinuum generation in suspended-core microstructured sulfide and tellurite optical fibers," Opt. Express **20,** 27083–27093 (2012).

8. M. Boivin, M. El-Amraoui, Y. Ledemi, S. Morency, R. Vallée, and Y. Messaddeq, "Germanate-tellurite composite fibers with a high-contrast step-index design for nonlinear applications," Opt. Mater. Express **4,** 1740–1746 (2014).
9. G. Tao, A. M. Stolyarov, and A. F Abouraddy, "Multimaterial Fibers," Int. J. Appl. Glass Sci. **3,** 349–368 (2012).
10. H. T. Munasinghe, A. Winterstein-Beckmann, C. Schiele, D. Manzani, L. Wondraczek, S. Afshar V., T. M. Monro, and H. Ebendorff-Heidepriem, "Lead-germanate glasses and fibers: a practical alternative to tellurite for nonlinear fiber applications," Opt. Mater. Express **3,** 1488–1503 (2013).
11. W. Gao, M. El-Amraoui, M. Liao, H. Kawashima, Z. Duan, D. Deng, T. Cheng, T. Suzuki, Y. Messaddeq, and Y. Ohishi, "Mid-infrared supercontinuum generation in a suspended-core As_2S_3 chalcogenide microstructured optical fiber," Opt. Express **21,** 9573–9583(2013).
12. X. Jiang, N. Y. Joly, M. A. Finger, F. Babic, G. K. L. Wong, J. C. Travers, and P. St. J. Russell, "Deep-ultraviolet to mid-infrared supercontinuum generated in solid-core ZBLAN photonic crystal fibre," Nature Photon. **9,** 133–139 (2015).
13. K. Clarke and Y. Ito, "Manufacture of fluoride glass preforms," J. Non-Cryst. Solids **140,** 265–268 (1992).
14. S. Mitachi, T. Miyashita, and T. Kanamori, "Fluoride-glass-cladded optical fibres for mid-infra-red ray transmission," Electron. Lett. **17,** 591–592 (1981).
15. R. J. Seyler, *Assignment of the glass transition,* STP 1249, (American Society for Testing and Materials, 1994).
16. G. L. Weissler and R. W. Carlson, *Methods of Experimental Physics. Vol. 14: Vacuum physics and technology,* (Academic Press, 1979).
17. E. B. Shand, *Glass engineering handbook,* (McGraw-Hill, 1958).
18. M. Idriss, F. Célarié, Y. Yokoyama, F. Tessier, and T. Rouxel, "Evolution of the elastic modulus of Zr-Cu-Al BMGs during annealing treatment and crystallization: Role of Zr/Cu ratio," J. Non-Cryst. Solids **421,** 35–40 (2015).
19. G. Roebben, B. Bollen, A. Brebels, J. Van Humbeeck, and O. Van der Biest, "Impulse excitation apparatus to measure resonant frequencies, elastic moduli, and internal friction at room and high temperature," J. Non-Cryst. Solids **68,** 4511–4515 (1997).
20. A. K. Varshneya and J. E. Marra, "Stresses in Dumet-Glass Seals," Physics **68,** 127–130 (1985).
21. H. Poritsky, "Analysis of Thermal Stresses in Sealed Cylinders and the Effect of Viscous Flow During Anneal," Physics **5,** 406–411 (1934).
22. K. Brugger, "Effect of Thermal Stress on Refractive Index in Clad Fibers," Appl. Opt. **10,** 437–438 (1971).
23. E. Le Bourhis, *Glass: Mechanics and Technology* (Wiley, 2014).
24. V. V. Dorofeev, A. N. Moiseev, M. F. Churbanov, G. E. Snopatin, A. V. Chilyasov, I. A. Kraev, A. S. Lobanov, T. V. Kotereva, L. A. Ketkova, A. A. Pushkin, V. V. Gerasimenko, V. G. Plotnichenko, A. F. Kosolapov, and E. M. Dianov, "High-purity TeO_2–WO_3–(La_2O_3, Bi_2O_3) glasses for fiber-optics," Opt. Mater. **33,** 1911–1915 (2011).
25. J. Massera, A. Haldeman, J. Jackson, C. Rivero-Baleine, L. Petit, and K. Richardson, "Processing of Tellurite-Based Glass with Low OH Content," J. Am. Ceram. Soc. **94,** 130–136 (2011).

1. Introduction

Broadband laser sources possessing the required characteristics to emit over the spectral range corresponding to the second atmospheric window (3 to 5 μm) exert a considerable attraction in diverse fields such as remote detection of atmospheric pollutants and infrared countermeasures [1–4]. Supercontinua generated inside optical fibers represent an interesting option to achieve this kind of laser sources. Indeed, they possess a high intensity, a broad spectral content, an excellent beam directionality, and a good potential to make robust and compact light sources [2, 5–7]. However, the generation of such supercontinuum involves some challenges in terms of optical fiber design. In fact, these optical fibers must show low propagation losses over the spectral range from 3 to 5 μm, possess a high nonlinear parameter and enable pumping in the anomalous dispersion regime at wavelengths for which compact laser sources are commercially available. In terms of robustness, these fibers must preferably show good mechanical properties and chemical stability against corrosion by moisture.

In our approach, germanate-tellurite composite fibers with a highly contrasted index step were designed to achieve visible to mid-infrared supercontinuum generation [8]. This type of fiber can be considered as multimaterial fibers [9]. Indeed, our fibers respectively combines the $69TeO_2 - 23WO_3 - 8La_2O_3$ (TWL) glass and the $47.5GeO_2 - 17.5TeO_2 - 20ZnO - 15Na_2O$ (GTZN) glass for its core and its cladding. This combination of glasses allows to obtain a difference of refractive index of about 0.33 between the core and the cladding of these fibers. Owing

to this high index step, these fibers can strongly confine the optical modes inside their core even when their core diameter approaches the value of the propagating light wavelength (λ). This enables them to achieve a small effective mode area (A_{eff}) and therefore to reach a high parameter of nonlinearity ($\gamma = [2\pi n_2]/[\lambda A_{eff}]$, where n_2 is the nonlinear refractive index of the core glass). Their high index step also allows to optimize their characteristics of chromatic dispersion for the generation of supercontinuum. In addition, their all-solid cross-section provides them with an improved stability against corrosion by ambient moisture and likely better mechanical properties compared to those demonstrated by microstructured optical fibers based on heavy metal oxide glasses, chalcogenide glasses and fluoride glasses [7, 10–12]. However, the fabrication of these composite fibers is complicated by the necessity of associating glasses whose thermomechanical properties match sufficiently together to allow them to be drawn into optical fibers.

In the first part of this work, a theoretical modeling is carried out to calculate the build-up of the thermal stress inside the composite preforms during their cooling toward ambient temperature once their annealing was accomplished. This thermal stress is mainly caused by the mismatch between the respective thermal expansion coefficients of the core and cladding glasses. This analysis brings out the counterbalancing of the tensile stress accumulated over the temperature range between the glass transition (T_g) and the strain point (T_s) by the compressive stress cumulated from T_s to ambient temperature. For the TWL-GTZN glass combination, this balancing of stress results in a moderate compressive stress on the cladding of the preform which makes possible its fabrication in a core-cladding configuration by the modified built-in casting technique described by Clarke *et al.* [13]. In the second part of this work, the results of supercontinuum (SC) generation inside TWL-GTZN composite fibers are shown. Since these fibers are composed of glasses that were synthesized under ambient air, the extent of their transmission spectrum in the mid-infrared is limited by strong absorption bands due to contamination of the glasses by hydroxyl (OH) groups. Despite this last inconvenience, the potential of these composite fibers for SC generation when they are pumped with a commercial thulium fiber laser can still be evaluated.

2. Experimental methods

2.1. Preparation and characterization of glasses

Glass samples were prepared by weighing and mixing metallic oxides and carbonates (purity $\geq$ 99.9 %) according to the molar ratios listed in table 1. Then, the powders were melted inside Pt/Au or gold crucibles at temperatures between 800 and 1000 °C under ambient air. This last preparation method was used both for bulk samples used to experimentally evaluate the thermal and mechanical parameters of each glass and for preform fabrication. Fabrication methods and optical characterization of the TWL-GTZN composite fibers were previously described elsewhere [8]. The initial core-cladding preform of the composite fiber was fabricated by using a modified built-in casting technique whose use allows the enhancement of the quality of the core-cladding interface compared to that achievable by the rod-in-tube technique [13, 14]. The preforms thus obtained were annealed at the T_g of the core glass during 4 h and were cooled down to room temperature (25 °C) at a rate of 1 °C/*min*. These preforms had an outer diameter of 10 mm, while their core, at their axial half-length, had a diameter around 6 mm. In fact, the size of the core varied from about 1 mm from one end to the other of the preforms due to the tapering of the inner diameter of the cladding tubes. This tapering had previously been caused during the fabrication process of the cladding tubes. The preforms had a total length of about 100 mm.

Table 1. Chemical compositions and thermal properties of the glasses used for the study of thermal stress inside composite preforms.

Acronyms	**Chemical compositions** (mol%)	T_g (°C)	T_x (°C)	ΔT (°C)
TWL (core)	$69TeO_2 - 23WO_3 - 8La_2O_3$	423	660	237
GTZNa	$45GeO_2 - 20TeO_2 - 20ZnO - 15Na_2O$	394	551	157
GTZN	$47.5GeO_2 - 17.5TeO_2 - 20ZnO - 15Na_2O$	401	565	164
GTZNb	$50GeO_2 - 15TeO_2 - 20ZnO - 15Na_2O$	413	571	158

Thermomechanical analyses (TMA) were carried out on glass samples shaped into rods having a diameter of 10 mm and a thickness around 5 mm. These samples were carefully annealed to avoid the presence of residual stresses inside their structure. TMA measurements were performed with a Netzsch TMA *F1 Hyperion* analyzer at a heating rate of 5 °C/min and a mechanical load of 0.02 N. The thermal expansion coefficients (α) of each glass were calculated from the slope of their respective TMA curve. The T_g and the T_s of each glass were also determined from the TMA curves. The T_g is defined as being located at the intersection of the extrapolations of the linear sections situated before and after the abrupt change of slope of the TMA curve [15]. The T_s corresponds to the temperature at which the TMA curve begins to diverge from its linear slope just before reaching the T_g [16, 17]. The onset of crystallization (T_x) of each glass was determined from differential scanning calorimetry (DSC) measurements acquired with a Netzsch DSC 404 *F3 Pegasus* calorimeter at a heating rate of 10 °C/min. The symbol ΔT refers to the difference between the respective T_x and T_g of each glass ($\Delta T = T_x - T_g$).

The Young's modulus (E) and the Poisson's ratio (ν) of each glass were measured over the temperature range from 50 °C to 450 °C by measuring their resonant frequency with an impulse excitation technique [18, 19]. This characterization was performed at a heating rate of 10 °C/min on disk-shaped samples having a diameter of 20 mm and a thickness around 2 mm.

2.2. Theoretical modeling of thermal stress inside optical fiber preforms

According to Varshneya *et al.* [20], the thermal stress (σ) inside two concentric cylinders with infinite lengths, of which the common interface is in perfect adhesion, and that are made from different materials, can be expressed as a function of radial position (r) in the following form:

$$\sigma_r = A + \frac{B}{r^2}, \tag{1}$$

$$\sigma_\theta = A - \frac{B}{r^2}, \tag{2}$$

$$\sigma_z = C, \tag{3}$$

where the values of A, B, and C for each material are interrelated through the equations

$$A_1 = A_2 R, \tag{4}$$

$$B_1 = 0, \tag{5}$$

$$C_1 = C_2 R, \tag{6}$$

$$R = 1 - \left(\frac{R_2}{R_1}\right)^2, \tag{7}$$

$$A_2 = \left[\frac{-\delta}{det(D)}\right]\left[\left(\frac{1+\nu_2}{E_2}\right) - R\left(\frac{1+\nu_1}{E_1}\right)\right], \tag{8}$$

$$B_2 = -A_2 R_2^2, \tag{9}$$

$$C_2 = \left[\frac{-\delta}{det(D)}\right]\left[\left(\frac{1+\nu_2}{E_2}\right)(2-R) - \left(\frac{1+\nu_1}{E_1}\right)R\right], \tag{10}$$

$$\delta = (\alpha_2 - \alpha_1)(T - T_q). \tag{11}$$

In equations (8) and (10), D is the matrix

$$D = \begin{bmatrix} \left(\frac{1+\nu_2}{E_2}\right)(2-R) - \left(\frac{1+\nu_1}{E_1}\right)R & R\left(\frac{1+\nu_1}{E_1}\right) - \left(\frac{1+\nu_2}{E_2}\right) \\ 2\left[R\left(\frac{\nu_1}{E_1}\right) - \frac{\nu_2}{E_2}\right] & \left(\frac{1}{E_2} - \frac{R}{E_1}\right) \end{bmatrix}. \tag{12}$$

Inside these last equations, T_q is the temperature at which there is no structural stress, $\alpha_{1,2}$ the thermal expansion coefficients, R_1 the radius of the inner cylinder, R_2 the radius of the outer cylinder, $E_{1,2}$ the Young's modulus, and $\nu_{1,2}$ the Poisson's ratios. The subscripts 1 and 2 indicate that the values are associated to the materials respectively constituting the inner and outer cylinders. By convention, tensile stress is denoted by positive values and compressive stress, by negative values.

2.3. Supercontinnum (SC) generation

Then, the composite fibers drawn from the TWL-GTZN preform were used for supercontinuum generation. These fibers were pumped with a thulium mode-locked fiber laser whose emission is centered at 1.91 µm (Brevity Basics +, Novae Laser). It produces light pulses with a full duration at half-maximum of about 500 fs at a repetition rate of 20 MHz to reach a peak power around 20 kW. The output of this laser source was collimated to obtain a free-space beam of 4 mm diameter. This beam was then injected inside the core of the composite fibers with an aspheric lens (focal length: 8 mm). The injection efficiency into the fibers was evaluated as being around 70 % by assuming propagation losses of 13 dB/m determined with the cut-back technique. The light was collected at the output of the composite fibers with a multimode fluoride fiber having a core diameter of 110 µm. Then, the collected light was analyzed on the spectral range from 600 nm to 3400 nm with three different optical spectrum analyzers (OSA) (Yokogawa, spectral ranges: OSA 1= 600 − 1700 nm , OSA 2= 1200 − 2400 nm, OSA 3= 1500 − 3400 nm).

3. Results and discussion

3.1. Quantitative analysis of the thermal stress build-up inside composite preforms

The build-up of thermal stress inside composite preforms upon their cooling toward ambient temperature was quantitatively evaluated by using the theoretical model described by Poritsky [21] and independently corrected by Brugger [22] and Varshneya *et al.* [20]. This model allows the calculation of the structural stress caused by the mismatch between the thermal expansion coefficients of two concentric cylinders based on different materials sealed together. During this study, three different compositions of cladding glass were associated to the TWL core glass to make a composite preform [Table 1]. Of these three quite similar compositions, only the GTZN glass was suitable to obtain a crack-free preform with the TWL glass by the modified built-in casting method. Both TWL-GTZNa and TWL-GTZNb combinations gave rise to

preform fracturing while cooling down to room temperature. To explain this experimental observation, the thermal stress on the surface of each preform was calculated by using the thermal and mechanical parameters of each glass [Figs. 1 and 2, Table 2]. These analyses were focused on the stress forming on the surface of the preforms because this area is the most susceptible to fracturing processes [23]. In addition, a ratio of 3:5 between the core and cladding diameters and a total preform diameter of 10 mm were assumed for all calculations.

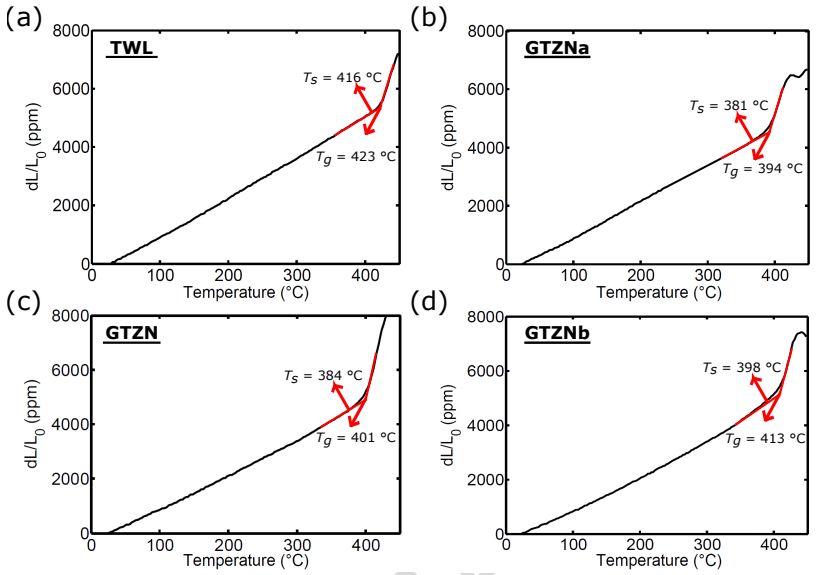

Fig. 1. TMA curves for the (a) TWL, (b) GTZNa, (c) GTZN, and (d) GTZNb glasses.

An example of stress analysis performed on the TWL-GTZN preform during its cooling toward ambient temperature is shown in Fig. 3. In each graph of this last figure, three temperature ranges are identified from I to III. These ranges correspond to three different dynamics of stress forming during preform cooling. The range I, at high temperature, starts at the T_g of the core glass which is slightly above the T_g of the cladding glass. On this interval of temperature, there is no stress inside the preform because the viscous behavior of the cladding glass allows the relaxation of the structural stress over a short period of time without altering its shape. The relaxation time varies from a few seconds at temperatures above T_g to tens of minutes at T_g [23]. The range II spreads from T_s to T_g. On this range of temperature, the relaxation time of the stress inside the cladding glass is of the order of a few hours [16]. For this analysis, it is considered that the cooling of the preform is fast enough so that the stress relaxation on this latter range cannot take place. The range III spreads from T_s to ambient temperature (25 °C). Over this range, the glass viscosity is sufficiently high that no relaxation can occur. The total stress inside the preform at ambient temperature can be calculated by summing the thermal constraints being formed over the temperature ranges II and III.

The thermal stress generated over the temperature ranges II and III comes from the mismatch between the respective thermal expansion coefficients of the cladding and core glasses [Table 2, Eq. (3)]. Over the range II, the coefficient of thermal expansion of the cladding glass ($\alpha^*_{\mathrm{GTZN}} = (32 \pm 1) \times 10^{-6}/°\mathrm{C}$) is higher than that of the core glass ($\alpha^*_{\mathrm{TWL}} = (14.8 \pm 0.1) \times 10^{-6}/°\mathrm{C}$). Consequently, a tensile stress is produced on the cladding of the preform during cooling. Over the range III, the situation is reversed: the coefficient of thermal expansion of the cladding glass ($\alpha_{\mathrm{GTZN}} = (12.8 \pm 0.1) \times 10^{-6}/°\mathrm{C}$) is lower than that of the core glass ($\alpha_{\mathrm{TWL}} =$

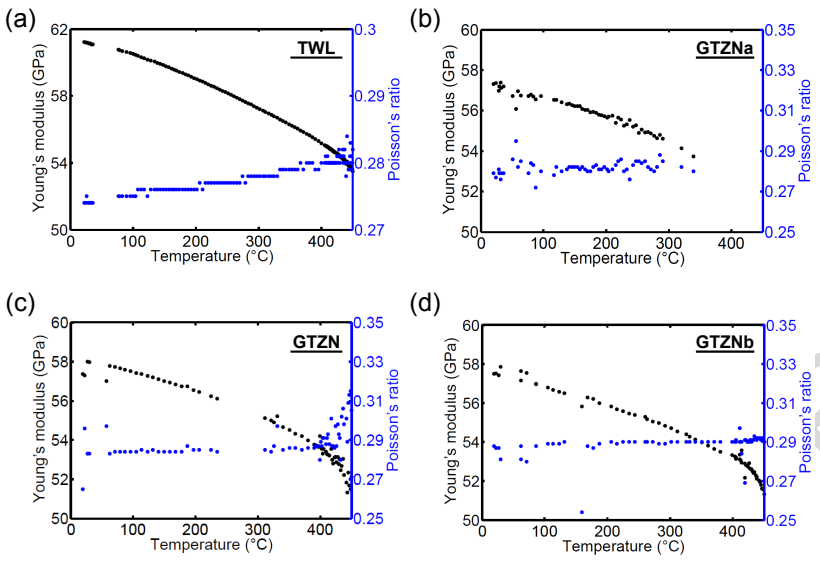

Fig. 2. Results of the impulse excitation analyses used to determine the Young's modulus and the Poisson's ratio of the (a) TWL, (b) GTZNa, (c) GTZN, and (d) GTZNb glasses.

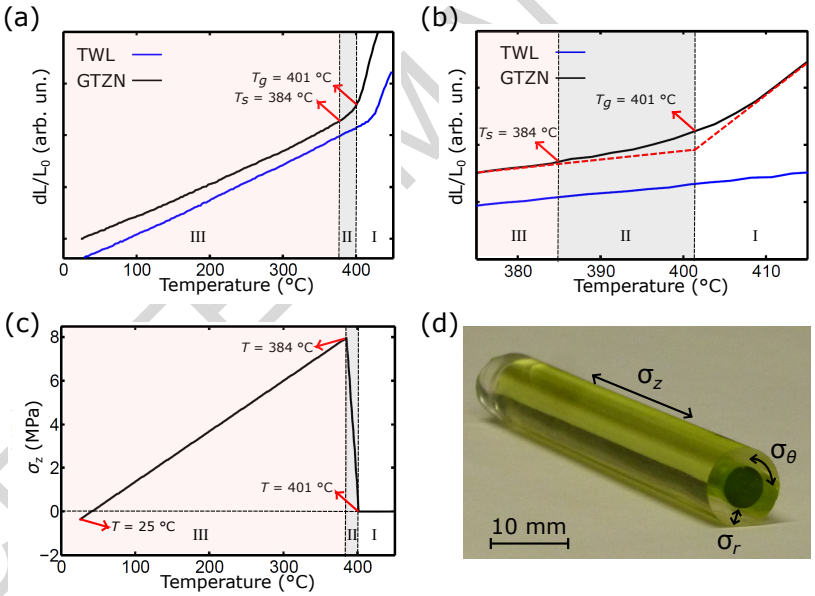

Fig. 3. Example of an analysis of the thermal stress performed for the TWL-GTZN preform. (a) Comparison between the TMA curves of the TWL and GTZN glasses. (b) Enlargement of the graph shown in (a) around the temperature range between the T_s and T_g of the cladding glass. (c) Axial stress (σ_z) inside the preform calculated from equation (3) as a function of temperature during its cooling toward ambient temperature. (d) Representation of the direction of each stress component inside the cladding of a TWL-GTZN preform (this image is a photograph of an actual TWL-GTZN preform).

$(13.6 \pm 0.1)\ \times 10^{-6}/^{\circ}\mathrm{C}$), a compressive stress is produced on the cladding during cooling toward ambient temperature. In this way, the accumulation of these tensile and compressive stresses can counterbalance each other and results in a preform showing moderate built-in stress once at ambient temperature [Fig. 3(c)].

Table 2. Thermal and mechanical parameters used for the theoretical modeling of the thermal stress inside the composite preforms. The mechanical parameters whose symbol is affixed with an asterisk means that their value corresponds to that measured over the temperature interval identified as the range II in Fig. 3 while those without asterisk are associated to range III. The Young's modulus (E) and Poisson's ratios (ν) listed in this table are average values over their corresponding temperature range.

Parameters	**TWL**	**GTZNa**	**GTZN**	**GTZNb**
T_s (°C)	416 ± 1	381 ± 1	384 ± 1	398 ± 1
T_g (°C)	423 ± 1	394 ± 1	401 ± 1	413 ± 1
α ($\times 10^{-6}/^{\circ}$C)	13.6 ± 0.1	12.4 ± 0.1	12.8 ± 0.1	13.0 ± 0.1
α* ($\times 10^{-6}/^{\circ}$C)	14.8 ± 0.1	28 ± 1	32 ± 1	39 ± 1
E (GPa)	59 ± 1	56 ± 1	57 ± 1	56 ± 1
E* (GPa)	55 ± 1	53 ± 1	54 ± 1	53 ± 1
ν	0.275 ± 0.005	0.280 ± 0.005	0.275 ± 0.005	0.290 ± 0.005
ν*	0.280 ± 0.005	0.280 ± 0.005	0.280 ± 0.005	0.290 ± 0.005

By using the parameters listed in table 2 and the theoretical model described by Varshneya *et al.* [Eq. (1), (2), and (3)] [20], the structural stress induced by cooling after annealing was calculated for each composite preform [Table 3]. The best equilibrium between the stresses cumulated over the temperature ranges II and III is achieved by the TWL-GTZN preform. In fact, the stress components on the external surface of its cladding at ambient temperature in the θ and z directions are evaluated as being both equal to (-0.3 ± 3.5) MPa. This last value represents an absolute minimum compared to those of the TWL-GTZNa and TWL-GTZNb preforms. The TWL-GTZNa preform shows a relatively high compressive stress on its cladding ($\sigma_\theta = (-7.4 \pm 3.5)$ MPa, $\sigma_z = (-7.6 \pm 3.5)$ MPa), while the TWL-GTZNb preform demonstrates a significant tensile stress ($\sigma_\theta = \sigma_z = (3.4 \pm 3.5)$ MPa). These last results thus explain why only the TWL-GTZN glass combination was able to experimentally produce a composite preform. However, the relatively large uncertainty of these results does not permit to conclude if the stress at ambient temperature on the cladding of the TWL-GTZN preform is in compression or in extension. Nevertheless, only a moderate compressive stress on the cladding of this preform can explain its good mechanical properties observed experimentally. Indeed, a compressive stress on the surface of a bulk glass inhibits growth of superficial cracks, thereby improving its mechanical strength [23]. The large uncertainty of these results of total stress calculations mainly comes from the subtraction between the cumulative stresses over the temperature ranges II and III, which are two relatively close numbers. The subtraction of two close numbers hampers the good management of the error in numerical calculation. In addition, note that σ_r is always null in table 3 because there is no mechanical constraint in the radial direction on the external surface of the preforms.

Table 3. Stress components on the surface of the cladding of the analyzed composite preforms once cooled to ambient temperature calculated from equations (1), (2) and (3) ($R_1/R_2 = 0.6$, $r = R_2 = 5$ mm, $T = 25$ °C).

Composite preforms	σ_r (MPa)	σ_θ (MPa)	σ_z (MPa)
TWL-GTZNa	0	-7.4 ± 3.5	-7.6 ± 3.5
TWL-GTZN	0	-0.3 ± 3.5	-0.3 ± 3.5
TWL-GTZNb	0	3.4 ± 3.5	3.4 ± 3.5

3.2. Supercontinnum (SC) generation inside GTZN-TWL composite fibers

As mentioned in the introduction, composite optical fibers had already been fabricated from TWL-GTZN preforms and these fibers possess interesting properties for the generation of non linear effects [8]. Figure 4(a) compares supercontinua produced inside TWL-GTZN fiber sections of 2 cm and 13 cm in length with similar pumping conditions. A wider spectral content was generated in the infrared when the shortest fiber section was used. Indeed, the spreading of the SC stops at 2.75 µm when the 2 cm fiber section was employed while it stops at 2.56 µm with the 13 cm fiber section. This last observation indicates that the spectral broadening of the SC seems to be limited by the absorption losses related to the hydroxyl (OH) bands [7]. These high losses were anticipated, since the glasses used for fiber fabrication were synthesized under ambient air and they consequently contain a strong concentration of OH groups due to contamination from ambient humidity. The OH absorption losses were evaluated to 1500 dB/m at 3.2 µm inside a bulk sample made of TWL core glass [8]. At 2.75 µm, these losses are measured as being equal to ∼500 dB/m. It is thus expected that the 2 cm fiber section produces a wider SC in the infrared since it generates absorption losses of 10 dB at 2.75 µm over its entire length which is lower than those of 65 dB produced by the 13 cm section. Consequently, it is preferable to use a short section of TWL-GTZN composite fiber for SC generation in order to prevent the spectral broadening from being too greatly limited by the OH absorption losses. To overcome this last problem, appropriate purification methods need to be implemented during the synthesis of the glasses constituting the composite fibers [7, 24, 25].

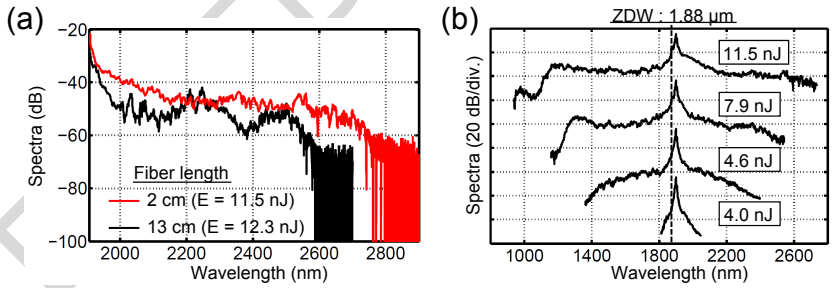

Fig. 4. (a) Comparison between the spectral contents of SC generated inside TWL-GTZN composite fiber sections of 2 cm and 13 cm in length. (b) Study of the spectral broadening of SC generated inside a 2 cm fiber section as a function of the incident energy per pulse. The zero dispersion wavelength (ZDW) of the composite fiber used in these experiments was calculated as being located at 1.88 µm (vertical dotted line).

Figure 4(b) shows the spectral width of the SC generated inside 2 cm of composite fiber as a function of the incident energy per pulse. At a pulse energy of 11.5 nJ, the maximum energy that the mode-locked laser source was able to emit during this experiment, the generated SC spreads from 1.1 to 2.75 µm into the infrared. The spectral broadening of the SC was facilitated

by the fact that the fiber was pumped into its anomalous dispersion regime near its zero dispersion wavelength (ZDW) located at 1.88 μm [8]. By using the required parameters for describing the pumping conditions ($\lambda = 1.91$ μm, $T_0 = T_{\mathrm{FWHM}}/[2\ln(1+\sqrt{2})] = 284$ fs) and light propagation inside the composite fiber ($\beta_2 = -8.7$ ps^{2}km^{-1}, $P_0 = 14$ kW, $\gamma = 174$ W^{-1}km^{-1}) [8], the characteristic dispersion length ($L_{\mathrm{D}} = T_0^2/|\beta_2|$) was calculated as being 9.2 m and the characteristic length of non-linearity ($L_{\mathrm{NL}} = [\gamma P_0]^{-1}$) as being 0.41 mm [5]. With these last characteristic lengths, the light pulse, at the beginning of its propagation inside the composite fiber, was calculated as being equivalent to a soliton of order $N = 151$ ($N = [L_{\mathrm{D}}/L_{\mathrm{NL}}]^{1/2}$). Such high order of soliton indicates that the initial spectral broadening of the SC was the consequence of the modulation instability (MI). Indeed, the soliton fission length ($L_{\mathrm{fiss}} \approx L_{\mathrm{D}}/N$) was 61 mm while the approximate length at which the spectral broadening due to MI becomes important ($L_{\mathrm{MI}} \approx 16L_{\mathrm{NL}}$) was 6.6 mm [5]. The MI was produced before soliton fission could occur. The SC generated in this way should possess a low temporal coherence since its initial dynamic of spectral broadening was initiated by the amplification of intrinsic optical noise overlapping the spectral bands of MI gain [5].

4. Conclusion

The build-up of thermal stress inside three different composite preforms during their cooling after annealing was analyzed with a theoretical model. This analysis has demonstrated that the TWL-GTZN preform is the one resulting in the lowest structural stress ($\sigma_\theta = \sigma_z = (-0.3 \pm 3.5)$ MPa) once at ambient temperature despite the appreciable dissimilarities between the thermal and thermomechanical properties of its core and cladding glasses. This study has thus enabled the establishment of a new rule for the fabrication of preforms with the modified built-in casting technique. This rule states that when two glasses show dissimilarities between their respective coefficient of thermal expansion, there is still the possibility to counterbalance the thermal stress caused by this last mismatch by that generated over the thermal range between the T_s and the T_g of the cladding glass. In specific conditions, this balancing can result in a moderate structural stress inside the preform once at ambient temperature that allows its further handling for fiber drawing. However, this last rule is only valid in cases where the T_g and the thermal expansion coefficient of the cladding glass are lower than those of the core glass. It might also be reversed for cases where the T_g and the thermal expansion coefficient of the cladding glass are higher than those of the core glass. In other words, the tensile stress generated over the thermal range below the T_s of the core glass could be compensated by the compressive stress produced between the T_s and the T_g of this same glass.

Then, the composite fibers previously drawn from the TWL-GTZN preforms were used for SC generation. With these composite fibers, a SC covering the spectral range from 1.1 to 2.75 μm was generated by pumping a 2 cm fiber section with a mode-locked fiber laser centered at 1.91 μm. The infrared extent of this SC was mainly limited by the absorption losses due to the high OH group concentration contained inside the glasses composing the fibers. These last results support the fabrication of composite fibers that would be made from glasses with low OH contents. Low-loss composite fibers would possess interesting properties for the generation of a SC whose spectral extension in the mid-infrared would be limited by the multiphonon absorption edge of tellurite glasses.

Acknowledgments

We acknowledge financial support from the Canada Excellence Research Chair (CERC) in Photonic Innovations, the Fonds de recherche du Québec - Nature et technologies (FRQNT), and the Canada Foundation for Innovation (CFI).